Ecological Complexity 34 (2018) 58–68

Contents lists available at ScienceDirect

Ecological Complexity

journal homepage: www.elsevier.com/locate/ecocom

Original research article

Assessing the characteristics of net primary production due to future climate change and CO_2 under RCP4.5 in China

Guodong Sun[a,c,*], Mu Mu[b]

[a] State Key Laboratory of Numerical Modeling for Atmospheric Sciences and Geophysical Fluid Dynamics (LASG), Institute of Atmospheric Physics, Chinese Academy of Sciences, Beijing 100029, China
[b] Fudan University, Shanghai 200433, China
[c] University of Chinese Academy of Sciences, Beijing 100049 China

ARTICLE INFO

Article history:
Received 28 November 2017
Revised 17 April 2018
Accepted 18 April 2018
Available online 5 May 2018

Keywords:
Net primary production
Prediction
Climate change
CNOP-P approach
Carbon cycle

ABSTRACT

In this study, the maximal extent of future net primary production (NPP) uncertainties are explored by employing the conditional nonlinear optimal perturbation related to parameters (CNOP-P) approach and the Lund-Potsdam-Jena (LPJ) model based on future climate change assessments, which are provided by 10 general circulation models (GCMs) of the Coupled Model Intercomparison Project 5 (CMIP5) under the Representative Concentration Pathway (RCP) 4.5 scenario at the North-South Transect of Eastern China (NSTEC). The CNOP-P approach produces a scenario of climate change within the feasible bounds that could cause maximal uncertainty of NPP. We find that the future NPP will increase due to changes in climate and atmospheric CO_2; however, there is a difference in the extent of the variation resulting from the 10 GCMs and the CNOP-P approach. Future NPPs are estimated from 3.89 Gt C (MRI-CGCM3 model) to 4.51 Gt C (bcc-csm1-1 model) using the LPJ model driven by the outputs of 10 GCMs. The estimates of NPP with two CNOP-P-type climate change scenarios are 4.74 Gt C and 5.31 Gt C and are larger than estimates of NPP by the outputs of the 10 GCMs. The above results imply that the terrestrial ecosystem supplies possible conditions for future carbon sinks for all climate change scenarios, especially for the CNOP-P-type climate change scenarios, although the estimates remain uncertain. Stimulative photosynthesis due to high precipitation and restrained autotrophic respiration due to low temperatures may play important roles in the carbon sink due to the CNOP-P-type climate change and CO_2 in all climate change scenarios. In addition, it is found that the combination of climate change and increasing CO_2 is the main driver of the increase of NPP.

1. Introduction

The net primary production (NPP), which quantifies the amount of atmospheric carbon fixed by plants and accumulated as biomass, is considered an important regulating factor in the global carbon cycle (Fang et al., 2001; Nemani et al., 2003; Gonsamo et al., 2013; Ni, 2013; Walker et al., 2015). Therefore, the spatial and temporal characteristics of the global and regional NPP have been paid attention due to concerns about the current and future behavior of the terrestrial carbon cycle (Woodward and Lomas, 2004; Doughty et al., 2015). Therefore, accurate estimates or predictions of the variation of the NPP are studied and discussed.

Despite observation data and numerical models, uncertainties in NPP are still not adequately estimated and predicted (Chen et al., 2000; Wang and Barrett, 2003; Zhou et al., 2013; Zhu and Zhuang, 2015). For example, Shao et al. (2016) employed a literature-based data set with 54 NPP estimates from 33 studies and found that the NPP in China's terrestrial ecosystems was 3.35 ± 1.25 Pg C yr^{-1} (mean $\pm$ SD) during 1901–2005 (most estimates were during 1981–2001), which was very close to the value from the outputs of the Multi-scale synthesis and terrestrial model intercomparison project (MsTMIP) conducted during 1981–2000 (3.36 ± 0.63 PgC yr^{-1}). Moreover, some of the sources of uncertainty (e.g., the spatiotemporal scales and land cover conditions) were also detected using the approach of classification and regression tree (CART) analysis. Gao and Liu (2008) employed five terrestrial ecosystem models to estimate the NPP. They found that the average NPP of different models was 2.864 Gt C in China; however, the NPP estimated by the five models ranged from 2.421 to 3.341 Gt C. The study implies that model error is a key

* Corresponding author at: State Key Laboratory of Numerical Modeling for Atmospheric Sciences and Geophysical Fluid Dynamics (LASG), Institute of Atmospheric Physics, Chinese Academy of Sciences, Beijing 100029, China.
E-mail address: sungd@mail.iap.ac.cn (G. Sun).

https://doi.org/10.1016/j.ecocom.2018.04.001
1476-945X/

factor in the calculation of NPP. In addition, the uncertainties of the feedback between vegetation and the atmosphere are also a main source of uncertainty in the estimates of NPP from the atmospheric general circulation model (AGCM) coupled with the terrestrial ecosystem model. Among all factors leading to uncertainties of the NPP using the terrestrial ecosystem models, the uncertainty of climate change is one of the key input factors for calculating the future NPP. Arora and Matthews (2009) calculated the NPP simulated by the box model equivalents of the Canadian Terrestrial Ecosystem Model (CTEM) and Top-down Representation of Interactive Foliage and Flora Including Dynamics (TRIFFID), forced with emissions from A2, A1B, and B1 IPCC SRES scenarios for the 2001–2100 period. Gang et al. (2015) utilized the modified Comprehensive Sequential Classification System (CSCS) model and 25 global climate models under the Representative Concentration Pathway 2.6 (RCP2.6) scenario to clarify the decadal variations of the NPP. All of the above studies found uncertainties of estimation of NPP in different climate change scenarios. Moreover, the response of NPP to climate change (temperature and precipitation) is nonlinear, further hindering exact calculations of NPP. Due to nonlinearity and relations between the terrestrial ecosystem and the atmosphere, current estimates of the NPP remain uncertain. Thus, the estimation of the range of the NPP under a reasonable climate change scenario is an interesting problem.

In this study, to reasonably estimate the variation of the NPP in future climate change scenarios and elucidate nonlinear relations between the NPP and climate change, the conditional nonlinear optimal perturbation related to parameters (CNOP-P) approach (Mu et al., 2010) is employed to estimate the maximal uncertainties of the NPP. CNOP-P represents a new climate change scenario, which is reasonably constrained by climate projections from 10 general circulation models (GCMs) of the Coupled Model Intercomparison Project 5 (CMIP5) under the Representative Concentration Pathway (RCP) 4.5 scenario. The CNOP-P approach has been widely applied to examine the uncertainties and predictability of atmosphere, ocean, and land processes, including the predictability of El Niño-Southern Oscillation (ENSO), typhoons, the Kuroshio large meander (KLM) state, grassland ecosystems (Duan and Zhang, 2010; Qin and Mu, 2011; Sun and Mu, 2011, 2014; Wang et al., 2012; Zheng et al., 2012), and terrestrial ecosystems. Moreover, Sun and Mu (2013) employed the CNOP-P approach to evaluate the variations of the NPP in response to increases of 2 °C in temperature and 20% in precipitation, with changes in the variability and variances of temperature and precipitation. In their studies, these authors attempted to determine the maximal uncertainty of the models of the NPP. However, their climate change scenario was restricted to only an increase in temperature and precipitation by 2 °C and 20%, respectively, which may be statistical results from the GCMs. Future projections from GCMs do not yield consistent extents of variation in temperature and precipitation. Under the climate change scenarios provided by GCMs, the maximal uncertainty of the NPP in China remains unknown. Therefore, the maximal uncertainty of estimates of the NPP was explored based on the multiple GCMs.

2. Study region, model, and methods

2.1. Study region

There is notable spatial heterogeneity in the distribution of the NPP in China. The NPP is low in Northwestern and Southwestern China and high in Northern and Southern China. The sensitive regions of impact of climate change on the NPP are located in Northern and Southern China. Thus, the area of the North-South Transect of Eastern China (NSTEC) was chosen as the region for our study. This region extends from Hainan Island to the northern border of China, ranging from longitude 108° to 118° E at latitudes less than 40° N and from longitude 118° to 128° E at latitudes equal to or greater than 40° N (Li et al., 2004; Sheng et al., 2011; Lu et al., 2013; Zhan et al., 2014). Because this region is located in the Monsoon Asia region, climate change and its influence on NPP are intense (Mu et al., 2008). Thus, it is necessary to demonstrate the response of the NPP on climate change in NSTEC.

Table 1
Ten GCMs from CMIP5.

Model Name	Model ID	Country of origin	Resolution (Lat. × Long.)
ACCESS1-0	M01	Australia	1.875° × 1.25°
CCSM4	M02	USA	1.25° × 0.9°
CNRM-CM5	M03	France	~1.4° × 1.4°
Fgoals-s2	M04	China	~2.81° × 1.66°
HadGEM2-AO	M05	Korea	1.875° × 1.25°
HadGEM2-CC	M06	United Kingdom	1.875° × 1.25°
IPSL-CM5A-MR	M07	France	2.5° × 1.25°
MIROC5	M08	Japan	~1.4° × 1.4°
MPI-ESM-LR	M09	Germany	1.875° × 1.875°
MRI-CGCM3	M10	Japan	1.125° × 1.125°

2.2. LPJ model and input data

The LPJ dynamical global vegetation model ("LPJ version 1") is employed in our study. The LPJ model can provide a representation of terrestrial vegetation dynamics and biogeochemical cycling using process-based coding (Sitch et al., 2003). The model includes ten plant functional types (PFTs) used to distinguish different photosynthetic (C3 vs. C4), phenological (deciduous vs. evergreen), and physiognomic (tree vs. grass) features. It employs the Farquhar-Collatz photosynthesis scheme to simulate realistic gross primary production (GPP) and plant respiration. Subtracting plant respiration from GPP gives the net primary production (NPP). The LPJ-DGVM used in this study has been intensively applied to explore the impact of climate change on the regional terrestrial ecosystem (Wu et al., 2014; Wang, 2014; Zhao and Wu, 2014). In addition, the LPJ model has been developed as an inversion method for the models LPJ-GUESS (Lund-Potsdam-Jena General Ecosystem Simulator), LPJ-Why (LPJ Wetland Hydrology), and LPJ-WHyMe (LPJ Wetland Hydrology and Methane) (Wania et al., 2009, 2010) to assess the terrestrial carbon cycle in different regions (Wolf et al., 2012; Manusch et al., 2014; Allen et al., 2016). Additionally, the LPJ model has also been coupled with climate change to evaluate the interaction between the terrestrial carbon cycle and the atmosphere (Yurova and Volodin, 2011; Willeit et al., 2014).

To evaluate the future variation of the NPP and its uncertainty, the data (precipitation, temperature, cloud cover, and wet day frequency) driving the LPJ model under the Representative Concentration Pathway (RCP) 4.5 scenario are shown in Table 1. These results were employed to drive the LPJ model during 2011–2100. Each of these models is a fully coupled atmosphere-ocean model operating at geographical grid resolutions between 2° and 6° and resolving vertical processes between 10 and 20 layers of both the atmosphere and the ocean. The outputs from the ten models were spatially interpolated to a 0.5° resolution and bias-corrected (based on 1961–1990 bias) with CRU TS2.1 climate data set (Mitchell and Jones, 2005). Additionally, a data set of atmospheric CO_2 concentrations from RCP4.5 during 2011–2100 was also essential (IPCC, 2013). Soil texture data were based on the Food and Agriculture Organization (FAO) soil data set (Zobler, 1986).

2.3. Conditional nonlinear optimal perturbation related to parameter (CNOP-P) approach

Not only was the future uncertainty of the NPP evaluated, but the possible maximal uncertainty of the NPP was also explored

during 2011–2100. To determine the possible maximal uncertainty of the NPP, the conditional nonlinear optimal perturbation related to parameter (CNOP-P) approach was applied (Mu et al., 2003). CNOP-P is a type of model parameter perturbation that could cause errors and uncertainties in maximal prediction and simulation with a certain constraint and at an optimal time (Duan and Zhang, 2010; Sun and Mu, 2016). The model parameters include physical parameters representing physical processes, forcing data, and so on. In this study, forcing temperature and precipitation data are considered model parameters to explore the possible maximal uncertainty of the NPP due to climate change in NSTEC (Sun and Mu, 2012, 2014). In previous studies, the CNOP-P approach has been employed (Sun and Mu, 2016). Similarly, CNOP-P is introduced in our studies for the convenience of the readers as follows.

Let the ordinary or partial differential equations be as follows:

$$\begin{cases} \dfrac{\partial U}{\partial t} = F(U,P) \quad U \in R^n,\ t \in [0,T] \\ U|_{t=0} = U_0 \end{cases} \tag{1}$$

where F is a nonlinear operator, and P are the model parameters, which include physical parameters and forcing parameters in Eq. (1). In this study, the temperature, precipitation, wet day frequency, and cloud cover in the LPJ model are considered the forcing parameters. Let M_τ be the propagator of the ordinary or partial differential equations from the initial time 0 to τ. u_τ is a solution of the ordinary or partial differential equations at time τ and satisfies $u(\tau) = M_\tau(u_0, p)$.

Let $U(T;\ U_0,\ P)$ and $U(T;U_0,P) + u(T;U_0,p)$ be the solutions of the ordinary or partial differential equations (1) with the forcing vectors P and $P+p$. p indicates the errors and perturbations related to the forcing parameters temperature and precipitation. $u(T;\ U_0,\ p)$ describes the variations of the reference state $U(T;\ U_0,\ P)$ caused by the superposition of the forcing parameters, temperature and precipitation, with the errors and perturbations p related to the forcing parameters. $u(T;\ U_0,\ p)$ satisfies:

$$\begin{cases} U(T;U_0,P) = M_T(U_0,P) \\ U(T;U_0,P) + u(T;U_0,p) = M_T(U_0,P+p) \end{cases}.$$

For the chosen norm $\|\|$, a perturbation p_δ is a CNOP-P if and only if

$$J(p_\delta) = \max_{p\in\Omega} J(p), \tag{2}$$

where

$$J(p) = \|M_T(U_0,P+p) - M_T(U_0,P)\| \tag{3}$$

and P is a reference state of the forcing parameters in Eq. (1), and p is the perturbation of the forcing parameters. $p \in \Omega$ is a constraint condition.

2.4. Experimental design

To discuss the response of NPP to climate change exclusively, the initial conditions for running the LPJ model were kept the same for all experiments. The initial conditions were provided through repeating years 1901–1930 of the CRU TS2.1 climate data set to run the LPJ model over 1000 years (Sitch et al., 2003). In this study, 12 climate change scenarios were applied to demonstrate the uncertainties of future NPP for 2011–2100. 10 climate change scenarios were supplied by 10 GCMs (Table 1) under the Representative Concentration Pathway (RCP) 4.5 scenario for 2011–2100. The other two climate change scenarios were provided by the CNOP-P approach. The optimization time is 90 years, and T represents 2100 in the Eq. (3).

The ability to estimate the maximal uncertainty of a simulation or prediction caused by forcing data (climate change) is a characteristic of the CNOP-P approach. Based on this ability, the CNOP-P approach was employed to provide two new climate change scenarios. The CNOP-P, which is a type of forcing error constrained by physical conditions $p \in \Omega$, could trigger the maximal departure relative to the reference state. Therefore, the new climate change scenarios provided by the CNOP-P approach are constrained by the 10 climate change scenarios from 10 GCMs. In contrast, the reference state P should also be determined. The reference state is obtained from the ensemble average of the forcing data (temperature and precipitation) sets from the 10 GCMs. Diverse constraint conditions were shown to supply the two climate change scenarios. One constraint condition was calculated by the following equation.

$$\min_k \{P_{ijk} - \bar{P}_{ij}\}_{k=1,10} \le p_{ij} \le \max_k \{P_{ijk} - \bar{P}_{ij}\}_{k=1,10}. \tag{4}$$

i, j, and k are the year from 2011 to 2100, month from 1 to 12, and ten models. p_{ij} is the temperature and precipitation perturbation series for different years and months. P_{ijk} is the temperature or precipitation series for different years, months, and models. $\bar{P}_{ij}$ is the ensemble average of the forcing data (temperature and precipitation) sets of the 10 GCMs for different years and months. Another constraint condition is calculated by the following equation:

$$\left|p_{ij}\right| \le \sqrt{\frac{1}{10}\sum_{k=1}^{10}(P_{ijk} - \bar{P}_{ij})^2}\ . \tag{5}$$

The CNOP-P computed on the basis of the reference state and Eq. (4) is considered a CNOP-P-M-type climate perturbation. This type of climate condition is called the CNOP-P-M-type climate change scenario. Another scenario, called the CNOP-P-V-type climate change scenario, was obtained on the basis of the reference state and Eq. (5).

To obtain the optimal value of Eq. (2), a gradient-free optimization algorithm (Differential Evolution, DE, Storn and Price, 1997) was employed to compute the CNOP-P. The DE algorithm could calculate non-differentiable and nonlinear cost function with good convergence properties. In our studies, the cost function about the terrestrial ecosystem carbon cycle with the LPJ model may be non-differentiable. The conventional optimization algorithm with the gradient information could be applied to solve the cost function. Hence, the DE algorithm is employed to solve the CNOP-P.

3. Results and analyses

3.1. Response of the NPP to future climate changes

To explore the spatial distribution of future NPP, 12 climate change scenarios and transient CO_2 under the RCP4.5 scenario were employed to run the LPJ model. Fig. 1 shows the spatial characteristics of the NPP for 2011–2100. It was found that the NPP due to the different climate change scenarios has similar spatial characteristics. In Southern and Northeastern China, the NPPs are higher than 1000 g C yr^{-1} m^{-2} for most climate change scenarios. In some cases, such as the CNOP-P-V, CNOP-P-M, and MIROC5 climate change scenarios, the NPPs are higher than 800 g C yr^{-1} m^{-2} in arid and semi-arid regions of Northeastern China. The total estimated NPP in the NSTEC ranges from 3.89 Gt C (MRI-CGCM3 model) to 4.51 Gt C (bcc-csm1-1 model) for all climate change scenarios originating from the output of 10 GCMs during 2011–2100. Total NPP for the NSTEC is estimated as 5.31 Gt C for the CNOP-P-M-type climate change scenario and 4.74 Gt C for the CNOP-P-V-type climate change scenario during 2011–2100 (Table 2), which are higher than the value of 2.74 Gt C from 1961 to 1990 for

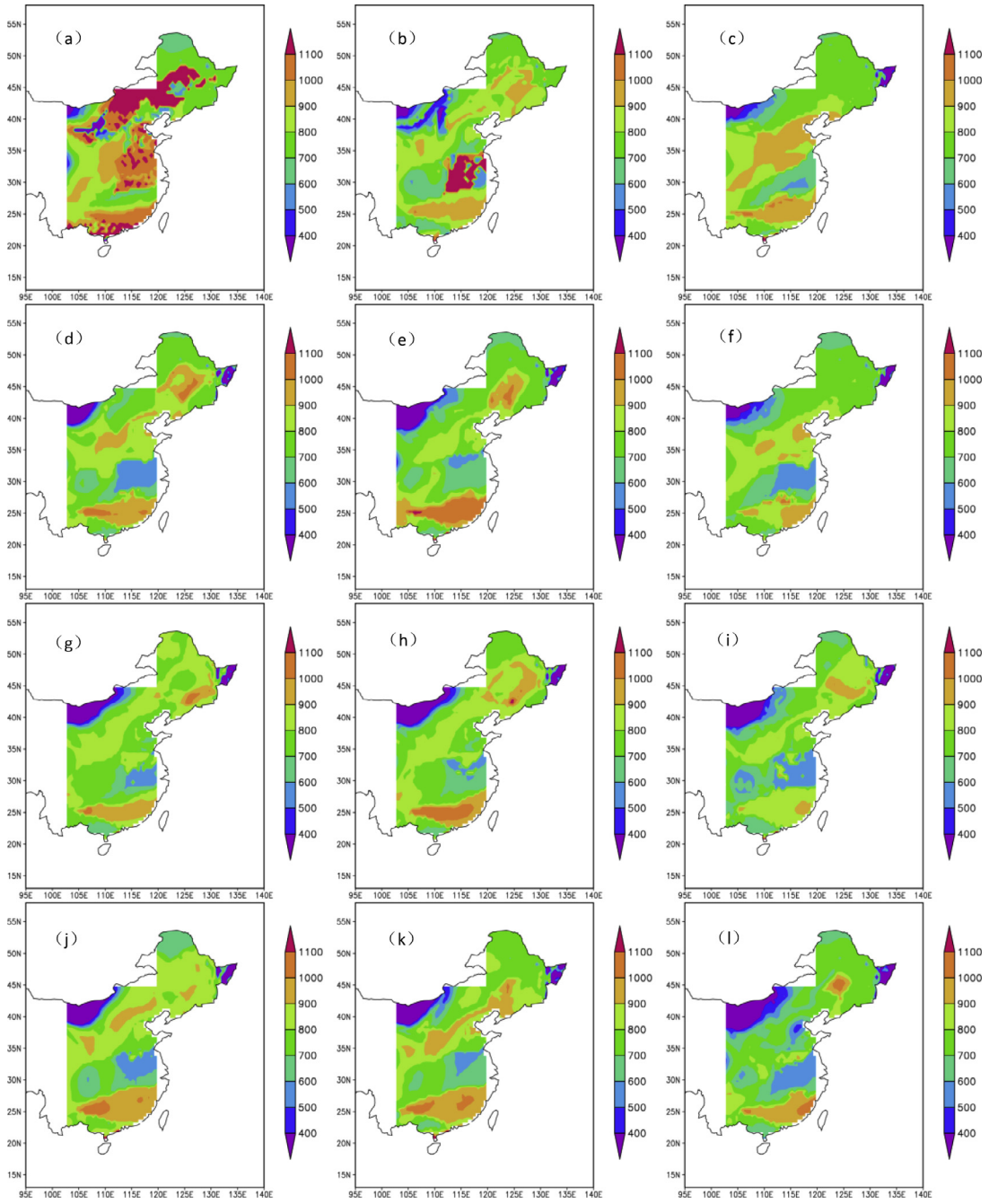

Fig. 1. Spatial distributions of averaged net primary production (NPP) from 2011 to 2100 driven by the CNOP-P-V-type and CNOP-P-M-type climate change scenarios and outputs from 10 GCMs. (a): CNOP-P-M-type climate change scenario; (b) CNOP-P-V-type climate change scenario; (c)-(l): ACCESS1-0, CCSM4, CNRM-CM5, Fgoals-s2, HadGEM2-AO, HadGEM2-CC, IPSL-CM5A-MR, MIROC5, MPI-ESM-LR, MRI-CGCM3 (Unit: g C m^{-2} $year^{-1}$).

the NSTEC using the LPJ model (Fig. 2). The largest value of NPP is obtained under the CNOP-P-M-type climate change scenario, compared with the other climate change scenarios, including the CNOP-P-V-type. These different variational features are obvious for the zonal mean of the NPP in different latitudes, i.e., from 19° to 24° N, from 29° to 35° N, and from 39° to 48°N (Fig. 3).

To explore the trend of the NPP in the study region, the interannual variations of NPP projected for the NSTEC for 10 climate change scenarios from GCMs and 2 climate change scenarios using the CNOP-P approach were evaluated (Fig. 4). It is shown that the NPP increases during 2011–2100 for all climate change scenarios. However, the extent of increase of NPP is different during 2011–2100 for all climate change scenarios. Furthermore, NPPs are shown in three different periods (2011–2040, 2041–2070, 2071–2100, Table 2–4) to explore their variations these periods. In the first 30 years, the fastest increase of the NPP is driven by the CNOP-P-M-type climate change scenario, and the average NPP is 4.99 Gt C during 2011–2040. NPP ranges from 3.68 (MRI-CGCM3 model) to 4.43 Gt C (bcc-csm1-1 model) during 2011–2040. In the following 60 years, nearly all NPPs show a persistent increase, showing a weak decrease only for the MIROC5 model. The above numerical results suggest that the NPP will increase.

Table 2
Main plant functional types and their total NPP during 2011–2040 under different climate change scenarios. (The number of grid in bracket).

Climate change scenario	Number of plant functional type and their NPP (Gt C)					Total (Gt C) (2011–2040)	Total (Gt C) (2011–2100)
	Temperate needle-leaved evergreen tree	Temperate broad-leaved evergreen tree	Temperate broad-leaved summer-green tree	Boreal needle-leaved evergreen tree	C3 perennial grass		
CNOP-P-Min-Max	0.41(190)	0.24(94)	1.47(668)	1.32(754)	1.49(692)	4.99	5.31
CNOP-P-Variance	0.15(97)	0.57(260)	1.29(701)	1.31(766)	1.06(586)	4.42	4.74
bcc-csm1-1	0.43(245)	0.39(176)	1.48(704)	1.82(1023)	0.26(234)	4.43	4.51
CCSM4	0.39(240)	0.43(190)	1.35(692)	1.33(765)	0.59(422)	4.18	4.43
CNRM-CM5	0.47(273)	0.47(186)	1.10(581)	1.41(841)	0.53(475)	4.04	4.27
FGOALS-g2	0.39(245)	0.35(163)	1.23(626)	1.85(1053)	0.36(293)	4.22	4.33
HadGEM2-AO	0.41(244)	0.40(177)	1.22(669)	0.62(367)	1.34(904)	4.05	4.31
HadGEM2-CC	0.47(264)	0.40(165)	1.12(600)	0.95(548)	0.93(719)	4.05	4.34
IPSL-CM5A-MR	0.25(186)	0.54(262)	1.16(648)	1.23(743)	0.58(482)	3.83	4.09
MIROC5	0.32(222)	0.61(259)	1.57(803)	0.71(411)	0.93(665)	4.19	4.41
MPI-ESM-LR	0.33(219)	0.60(263)	1.23(625)	1.66(905)	0.32(338)	4.21	4.40
MRI-CGCM3	0.43(258)	0.36(152)	1.07(624)	1.24(768)	0.54(500)	3.68	3.89

Table 3
Main plant functional types and their total NPP during 2041–2070 under different climate change scenarios. (The number of grid in bracket).

Climate change scenario	Number of plant functional type and their NPP (Gt C)					Total (Gt C) (2041–2070)
	Temperate needle-leaved evergreen tree	Temperate broad-leaved evergreen tree	Temperate broad-leaved summer-green tree	Boreal needle-leaved evergreen tree	C3 perennial grass	
CNOP-P-Min-Max	0.35(190)	0.31(110)	1.81(760)	1.41(780)	1.40(526)	5.42
CNOP-P-Variance	0.15(96)	0.60(260)	1.95(959)	1.15(644)	0.93(426)	4.88
bcc-csm1-1	0.34(211)	0.42(180)	1.69(766)	1.77(996)	0.18(139)	4.52
CCSM4	0.39(247)	0.46(190)	1.71(815)	1.18(620)	0.65(400)	4.52
CNRM-CM5	0.52(294)	0.48(184)	1.32(648)	1.31(716)	0.57(401)	4.35
FGOALS-g2	0.38(241)	0.38(165)	1.42(676)	1.90(1093)	0.18(134)	4.36
HadGEM2-AO	0.35(219)	0.41(179)	1.69(849)	0.20(105)	1.58(913)	4.36
HadGEM2-CC	0.44(263)	0.42(168)	1.68(804)	0.69(363)	1.03(643)	4.44
IPSL-CM5A-MR	0.27(191)	0.58(262)	1.51(772)	0.84(475)	0.90(582)	4.17
MIROC5	0.34(213)	0.64(260)	2.46(1172)	0.43(241)	0.57(410)	4.52
MPI-ESM-LR	0.36(222)	0.65(268)	1.46(715)	1.53(797)	0.26(265)	4.40
MRI-CGCM3	0.44(280)	0.37(152)	1.33(702)	1.25(697)	0.48(378)	3.96

Table 4
Main plant functional types and their total NPP during 2071–2100 under different climate change scenarios. (The number of grid in bracket).

Climate change scenario	Number of plant functional type and their NPP (Gt C)					Total (Gt C) (2071–2100)
	Temperate needle-leaved evergreen tree	Temperate broad-leaved evergreen tree	Temperate broad-leaved summer-green tree	Boreal needle-leaved evergreen tree	C3 perennial grass	
CNOP-P-Min-Max	0.35(192)	0.38(131)	1.87(790)	1.40(758)	1.37(488)	5.52
CNOP-P-Variance	0.16(98)	0.64(274)	2.06(1007)	1.13(624)	0.76(348)	4.93
bcc-csm1-1	0.35(209)	0.43(179)	1.88(869)	1.62(895)	1.83(141)	4.59
CCSM4	0.40(250)	0.47(190)	1.91(914)	1.08(559)	0.61(355)	4.60
CNRM-CM5	0.50(288)	0.48(183)	1.55(759)	1.08(575)	0.64(419)	4.43
FGOALS-g2	0.36(237)	0.40(170)	1.51(726)	1.92(1081)	0.11(77)	4.42
HadGEM2-AO	0.35(217)	0.42(181)	2.17(1035)	0.20(99)	1.21(696)	4.52
HadGEM2-CC	0.43(262)	0.42(166)	1.84(905)	0.53(268)	1.10(604)	4.55
IPSL-CM5A-MR	0.26(178)	0.58(267)	1.72(883)	0.78(419)	0.81(481)	4.26
MIROC5	0.32(197)	0.65(266)	2.48(1216)	0.40(224)	0.47(366)	4.51
MPI-ESM-LR	0.37(222)	0.66(267)	1.66(775)	1.44(733)	0.22(208)	4.59
MRI-CGCM3	0.41(261)	0.38(154)	1.51(788)	1.19(641)	0.42(352)	4.03

3.2. Variations in NPP for the primary PFTs

The distribution of vegetation changes due to climate change during the study period. At the same time, the NPPs related to the different plant functional types (PFTs) also undergo variations. To explore the variations of the PFTs and the NPP, vegetation amounts denoted as the number of grids, and their corresponding NPPs for three periods (2011–2040, 2041–2070, 2071–2100) are shown in Tables 2–4. It is found that temperate needle-leaved evergreen trees, temperate broad-leaved evergreen trees, temperate broad-leaved summergreen trees, boreal needle-leaved evergreen trees, and C3 perennial grass are the main PFTs during the study period in the NSTEC. Among the five PFTs, temperate broad-leaved summergreen trees, boreal needle-leaved evergreen trees, and C3 perennial grass occupy most of the study region. For example, temperate broad-leaved summergreen trees for different climate change scenarios occupy grids 581 (CNRM-CM5 model) to 803 (MIROC5 model), and the corresponding NPPs are from 1.07 Gt C (MRI-CGCM3 model) to 1.57 Gt C (MIROC5 model) during 2011–2040. Boreal needle-leaved evergreen trees occupy grids 367

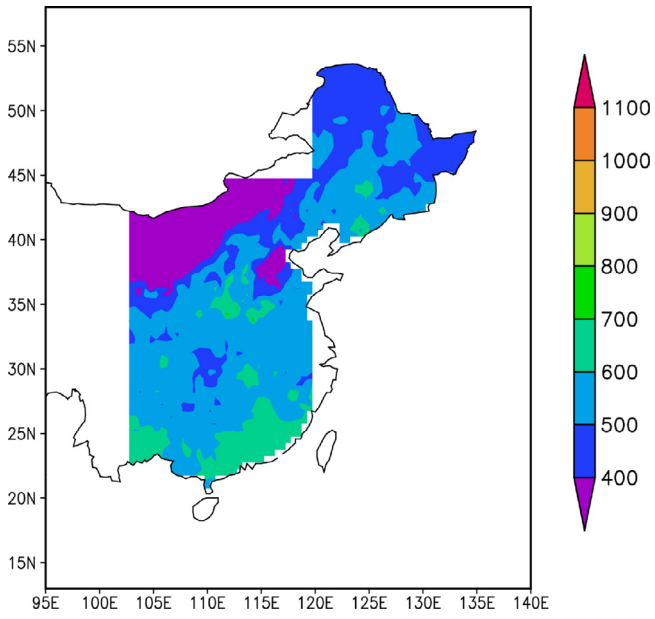

Fig. 2. Spatial distributions of averaged net primary production (NPP) from 1961 to 1990.

(HadGEM2-AO model) to 1053 (FGOALS-g2 model) for different climate change scenarios, and the corresponding NPPs are from 0.62 Gt C (HadGEM2-AO model) to 1.85 Gt C (FGOALS-g2 model) during 2011–2040. However, C3 perennial grass shows different characteristics. For most climate change scenarios, C3 perennial grass occupies larger grids, from 422 (CCSM4 model) to 904 (HadGEM2-AO model), and the corresponding NPPs are from 0.53 Gt C (CNRM-CM5 model) to 1.49 Gt C (CNOP-P-M-type climate change scenarios) during 2011–2040. The estimated grid numbers and NPPs of the bcc-csm1-1, FGOALS-g2, and MPI-ESM-LR models are small during 2011–2040. Similar results are obtained for the periods 2041–2070 and 2071–2100. From the distribution and corresponding NPP, it is found that the increasing grid number and NPP of C3 perennial grass may be the main characteristic of the CNOP-P-M-type climate change scenario.

4. Discussion

4.1. Variations of gross primary production and autotrophic respiration for different climate changes

Terrestrial NPP is defined as the difference between photosynthesis (gross primary productivity, GPP) and autotrophic

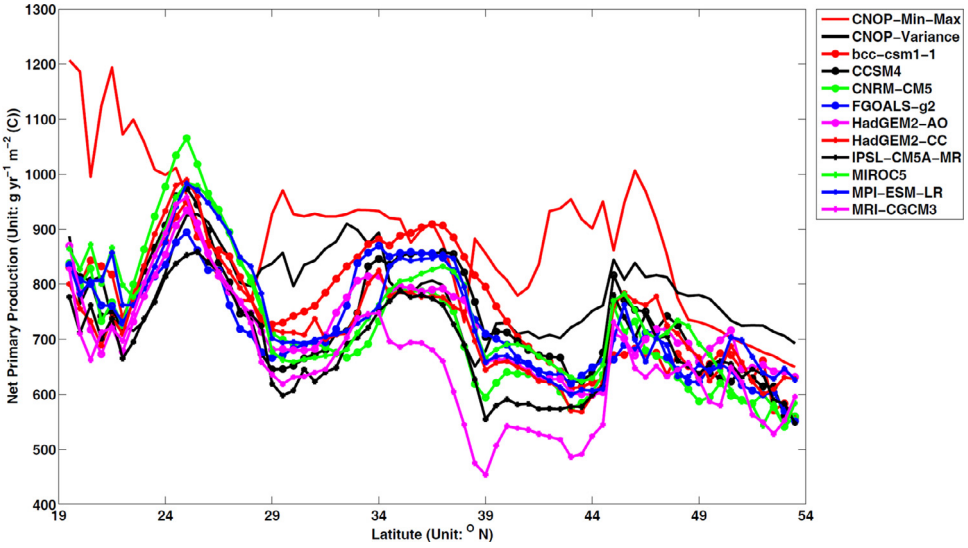

Fig. 3. Zonal averaged NPPs from 2011 to 2100 for different climate change scenarios.

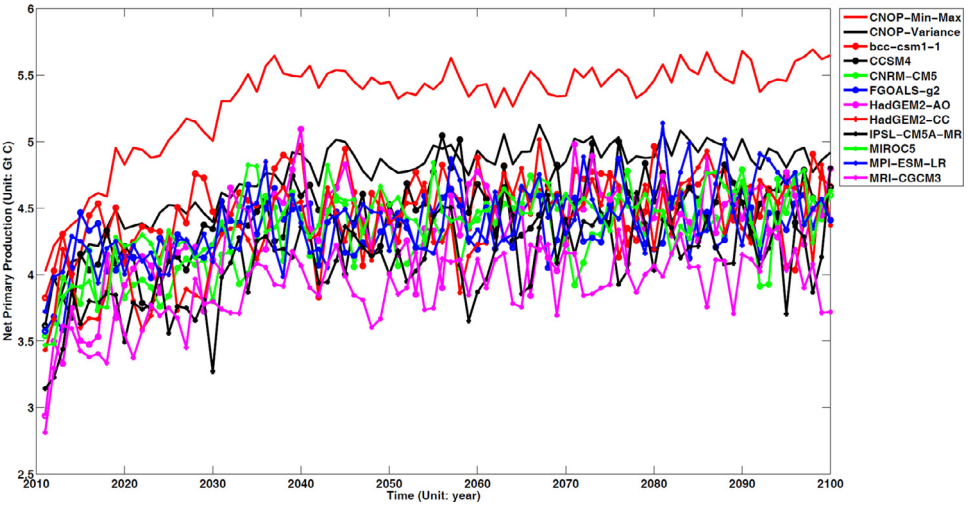

Fig. 4. Variations of NPP during 2011–2100 for different climate change scenarios.

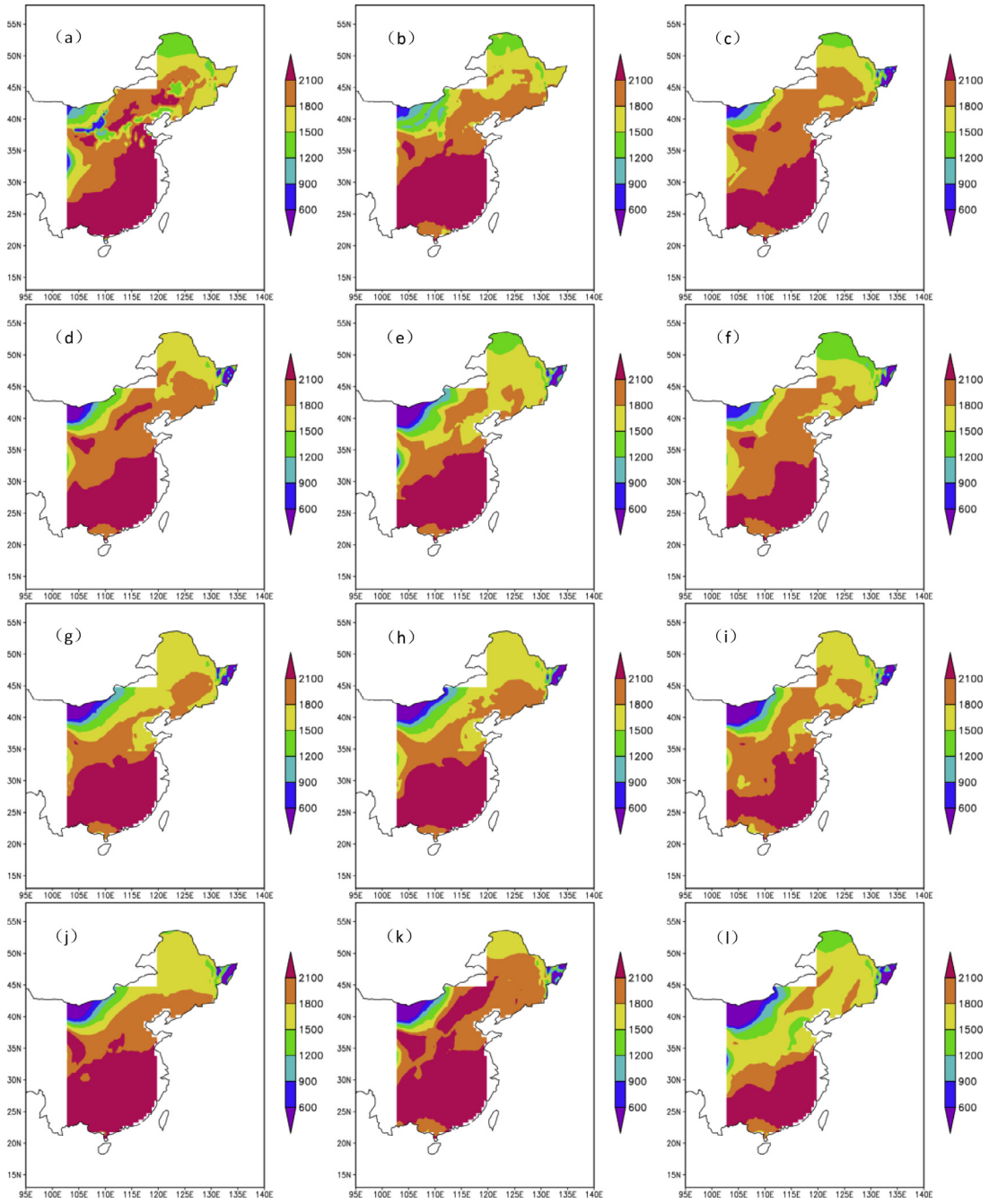

Fig. 5. Spatial distributions of averaged gross primary production (GPP) from 2011 to 2100 driven by the CNOP-P-V-type and CNOP-P-M-type climate change scenarios and outputs from 10 GCMs. (a): CNOP-P-M-type climate change scenario; (b) CNOP-P-V-type climate change scenario; (c)–(l): ACCESS1-0, CCSM4, CNRM-CM5, Fgoals-s2, HadGEM2-AO, HadGEM2-CC, IPSL-CM5A-MR, MIROC5, MPI-ESM-LR, MRI-CGCM3 (Unit: g C m^{-2} $year^{-1}$).

respiration (Ra). To discuss the possible reason for the different variations of the NPP for different climate change scenarios, the GPP and the Ra were explored for all climate change scenarios, with the spatial distributions shown in Figs. 5 and 6. Among all climate change scenarios, it is found that increasing precipitation promotes plant photosynthesis, especially in arid and semi-arid regions in China, such as in the CNOP-P-M-type and CNOP-P-V-type climate change scenarios, and ACCESS1-0, CCSM4, Fgoals-s2, MIROC5, and MPI-ESM-LR models. The increasing extent of the NPP for the CNOP-P-M-type climate change scenario is greatest among those variations for other climate change scenarios. In arid and semi-arid regions, the precipitation is scanty. Increasing precipitation favors plant photosynthesis and augments GPP. However, the low temperature restrains autotrophic respiration in the region. The above results demonstrate that stimulative photosynthesis and restrained autotrophic respiration lead to the increase of NPP. Besides arid and semi-arid regions in China, the NPP also increases in the Southern China, such as in the CNOP-P-M-type climate change scenario, and CNRM-CM5, HadGEM2-CC, MIROC5, and MPI-ESM-LR models. In the Southern China, precipitation is abundant and leads to augment of the GPP, and temperature also leads to augment of the Ra. However, the increasing extent of the Ra is less than that of the GPP. Finally, the NPP increases due to the minute increase of Ra relative to the increase of GPP.

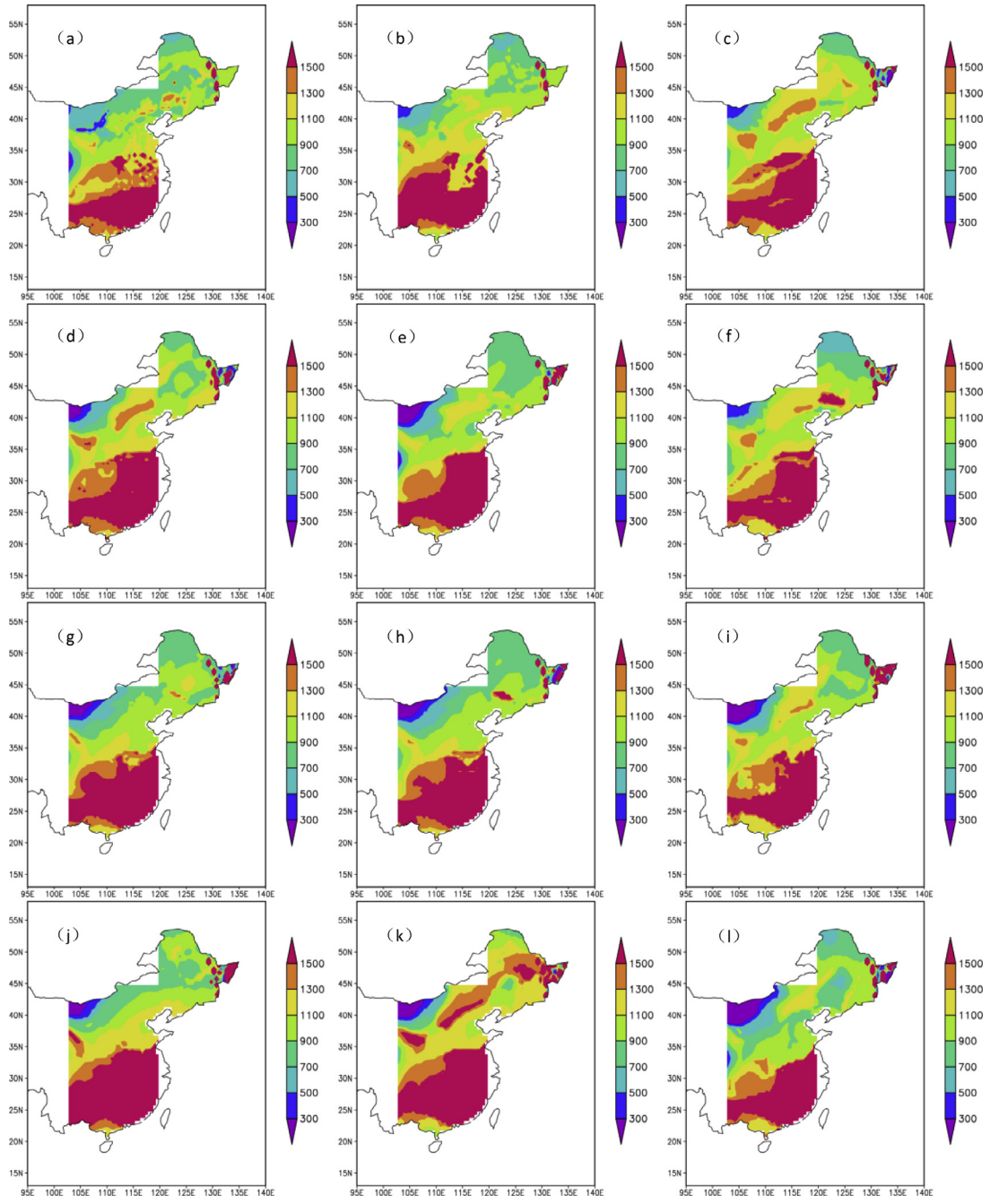

Fig. 6. Spatial distributions of averaged autotrophic respiration from 2011 to 2100 driven by the CNOP-P-V-type and CNOP-P-M-type climate change scenarios and outputs from 10 GCMs. (a): CNOP-P-M-type climate change scenario; (b) CNOP-P-V-type climate change scenario; (c)-(l): ACCESS1-0, CCSM4, CNRM-CM5, Fgoals-s2, HadGEM2-AO, HadGEM2-CC, IPSL-CM5A-MR, MIROC5, MPI-ESM-LR, MRI-CGCM3 (Unit: g C m^{-2} $year^{-1}$).

4.2. Estimates of NPP in different studies

It is important and interesting to compare different studies estimating NPP in China. There are several studies discussing the magnitude and uncertainty of the NPP in China. For example, Shao et al. (2016) summarized 54 estimates of the NPP from 37 studies, according to the literature-based data set. They found that the NPP in China's terrestrial ecosystems was 3.35 ± 1.25 Pg C yr_1 (mean ± SD) during 1901–2005. In our study, the average estimate of NPP was 2.74 Gt C from 1961 to 1990 for only the NSTEC region using the LPJ model. The estimates of the NPP from their studies are greater than those from our calculations because the study regions are different.

However, the projected estimates of the NPP have also been explored in China. Tao and Zhang (2010) used the LPJ model to show the increase in NPP over the period of 2011–2100, with eight future climate scenarios consisting of combinations of two GCMs and four IPCC SRES emission scenarios (A1FI, A2, B1, B2). At the end of the 21st century, NPP is estimated to be approximately 4.5 to 6 Gt C. In addition, Ji et al. (2008) also predicted future NPP using an atmosphere-vegetation interaction model (AVIM2). They found that the simulated total NPP in China would increase gradually for changing CO_2 B2. It will reach 3.99 Gt C in 2100, showing an increase of 35.7%. The above results indicate that the fertilization effects of increased CO_2 levels and the physiological and phenological effects of temperature-increase are the main

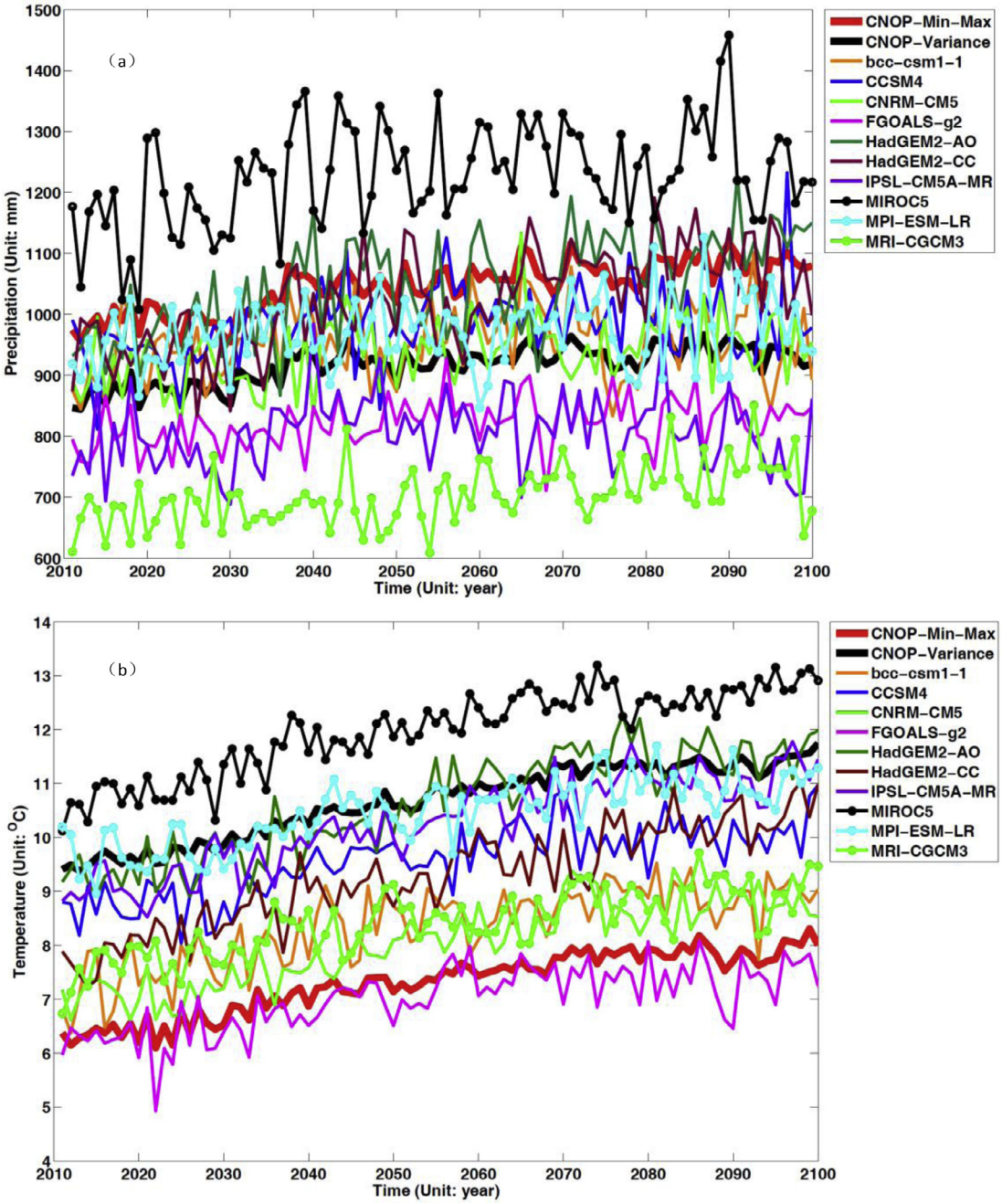

Fig. 7. Various climate change scenarios during 2011–2100. (a): Precipitation; (b): Temperature.

reasons. Additionally, the increase in precipitation in arid and semi-arid regions of China also contributes to the increase in NPP. Their findings are consistent with our research.

4.3. Interactions between NPP and climate change

Variations of the NPP as an important component of the global carbon cycle are strongly related to the climate change, primarily through temperature changes and water availability (Michaletz et al., 2014; Poulter et al., 2014). In our studies, it is found that the NPP increases for all climate change scenarios. Among all climate change scenarios, the extent of increase of NPP is the largest for the CNOP-P-M-type climate change scenario. High precipitation and low temperature characteristics are found under the CNOP-P-M-type climate change scenario. High precipitation may favor the GPP. The low temperature restrains plant respiration. Finally, the maximum extent of the NPP occurs under the CNOP-P-M-type climate change scenario. Although the high precipitation in the MIROC5 model (Fig. 7a) enhances the photosynthesis, the high temperature also promotes plant respiration (Fig. 7b). However, the low temperature restrains plant respiration in the FGOALS-g2 model (Fig. 7b). However, the precipitation is low and controls the photosynthesis. Thus, the variations of the NPP for the above two climate change scenarios are lower than that for the CNOP-P-M-type climate change scenario.

4.4. Relations between NPP, climate change, and CO_2

Variations of the NPP are dependent not only on climate change (Lucht et al., 2002; Nemani et al., 2003; Zhao and Running, 2010;

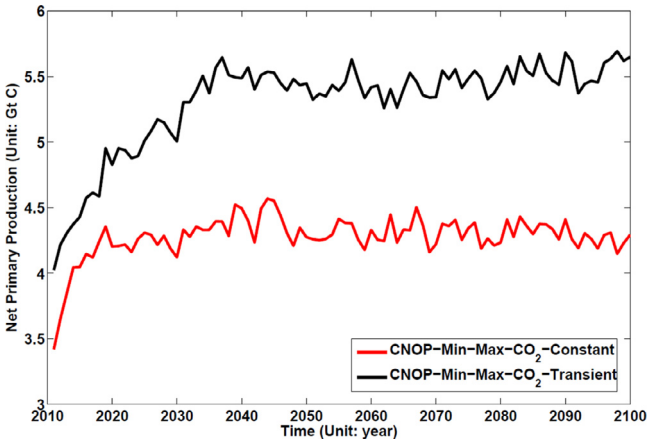

Fig. 8. Variations of NPP during 2011–2100 under the CNOP-P-M-type climate change scenarios, with and without increasing CO_2.

Tao and Zhang, 2010) but also on atmospheric CO_2 (DeLucia et al., 2005; Graven et al., 2013; Walker et al., 2015). To investigate the different responses of the NPP to CNOP-P-M-type climate change and CO_2, two groups of experiments were implemented. One experiment was conducted for the transient CO_2 concentration under the CNOP-P-M-type climate change scenario. The other experiment was carried out with the CO_2 concentration maintained at a constant level under the CNOP-P-M-type climate change scenario. It was found that the NPP with a transient CO_2 concentration is larger by 1.2 Gt C than that with a constant CO_2 concentration (Fig. 8) from 2011 to 2100. The numerical results suggest that CNOP-P-M-type climate change could augment NPP in the study region. However, CO_2 could promote the persistent increase. When the CO_2 concentration is restricted at a constant level, CNOP-P-M-type climate change leads to the steady interannual variation of the NPP. The increasing trend of the NPP is observed when CNOP-P-M-type climate change is combined with the transient CO_2 concentration, especially in the first 30 years. This implies that only CNOP-P-M-type climate change results in the interannual variation of the NPP. However, the combination of CO_2 concentration and the CNOP-P-M-type climate change could lead to variations in the trend. This also indicates that CO_2 concentration plays a key role in the variation of the NPP and the carbon source or carbon sink. Ji et al. (2008) also conducted similar numerical experiments. They implied that the NPP for constant CO_2 was smaller than that for changing CO_2 under B2 scenarios. This work and their work emphasize the fertilization effects of increasing CO_2 for plant growth.

5. Conclusion

The spatial and temporal variations of the future NPP are discussed using 10 climate change scenarios from GCMs and two CNOP-P-type climate change scenarios with the LPJ model and medium-low Representative Concentration Pathways (RCPs) in the NSTEC region. Compared to the NPP during 1961–1990, future NPP is estimated to increase during 2011–2100, according to 12 climate change scenarios. Among all climate change scenarios, CNOP-P-M-type climate change could cause the largest extent of increase in NPP (5.31 Gt C). Additionally, CNOP-P-M-type climate change was constrained by climate change conditions from 10 GCMs. This indicates that CNOP-P-M-type climate change scenario is reasonable, and supplies a possible upper bound of the estimated NPP. The numerical results suggest that plants in the NSTEC region might play the role of a carbon sink. The variation in plant functional types (PFTs) and the associated NPP shows similar characteristics under the 12 climate change scenarios provided by 10 GCMs and the CNOP-P approach. The numbers of grids of temperate broad-leaved summer-green trees, boreal needle-leaved evergreen trees, and C3 perennial grasses increase, and the associated NPP for each PFT also increases for most climate change scenarios.

Acknowledgment

Grants from the National Natural Science Foundation of China (Nos. 41675104, 91437111, 41375111) and Youth Innovation Promotion Association, Chinese Academy of Sciences (No. 2015060) provided funding for this research.

References

Allen, K.A., Lehsten, V., Hale, K., 2016. Past and future drivers of an unmanaged carbon sink in European temperate forest. Ecosystems 19, 545. doi:10.1007/s10021-015-9950-1.
Arora, V.K., Matthews, H.D., 2009. Characterizing uncertainty in modeling primary terrestrial ecosystem processes. Global Biogeochem. Cycles 23, GB2016. doi:10.1029/2008GB003398.
Chen, W., Chen, J., Liu, J., Cihlar, J., 2000. Approaches for reducing uncertainties in regional forest carbon balance, Global Biogeochem. Cycles 14 (3), 827–838. doi:10.1029/1999GB001206.
DeLucia, E.H., Moore, D.J., Norby, R.J., 2005. Contrasting responses of forest ecosystems to rising atmospheric CO_2: Implications for the global C cycle. Global Biogeochem. Cycles 19, GB3006. doi:10.1029/2004GB002346.
Doughty, C.E., et al., 2015. Drought impact on forest carbon dynamics and fluxes in Amazonia. Nature 519, 78–84.
Duan, W., Zhang, R., 2010. Is model parameter error related to a significant spring predictability barrier for El Nino events? Results from a theoretical model. Adv. Atmos. Sci. 27 (5), 1003–1013. doi:10.1007/s00376-009-9166-4.
Fang, J.Y., Piao, S.L., Tang, Z.Y., Peng, C.H., Ji, W., 2001. Interannual variability in net primary production and precipitation. Science 293 (5536), 1723. doi:10.1126/science.293.5536.1723a.
Gao, Z., Liu, J., 2008. Simulation study of China's net primary production. Chin. Sci. Bull. 53, 434. doi:10.1007/s11434-008-0097-8.
Gang, C., Wang, Z., Zhou, W., et al., 2015. Projecting the dynamics of terrestrial net primary productivity in response to future climate change under the RCP2.6 scenario. Environ. Earth Sci. 74, 5949. doi:10.1007/s12665-015-4618-x.
Gonsamo, A., Chen, J.M., Price, D.T., Kurz, W.A., Liu, J., Boisvenue, C., Hember, R.A., Wu, C., Chang, K.-H., 2013. Improved assessment of gross and net primary productivity of Canada's landmass. J. Geophys. Res. Biogeosci. 118, 1546–1560. doi:10.1002/2013JG002388.
Graven, H., Keeling, R., Piper, S., Patra, P., Stephens, B., Wofsy, S., Welp, L., Sweeney, C., Tans, P., Kelley, J., et al., 2013. Enhanced seasonal exchange of CO_2 by northern ecosystems since 1960. Science 341, 1085–1089.
IPCC, 2013. Climate change 2013: the physical science basis. In: Stocker, T.F., Qin, D., Plattner, G.-K., Tignor, M., Allen, S.K., Boschung, J., Nauels, A., Xia, Y., Bex, V., Midgley, P.M. (Eds.), Contribution of Working Group I to the Fifth Assessment Report of the Intergovernmental Panel on Climate Change. Cambridge University Press, Cambridge, United Kingdom and New York, NY, USA, p. 1535.
Ji, J.J., Huang, M., Li, K.R., 2008. Prediction of carbon exchanges between China terrestrial ecosystem and atmosphere in 21st century. Sci. China Ser. D 6, 885–898.
Li, Y., Liao, S., Chi, G., Liao, Q., 2004. NPP distribution related to the terrains along the North-South Transect of Eastern China. Chin. Sci. Bull. 49 (6), 617–624.
Lu, N., Sun, G., Feng, X., Fu, B., 2013. Water yield responses to climate change and variability across the North–South Transect of Eastern China (NSTEC). J. Hydrol. 481, 96–105.
Lucht, W., Prentice, I.C., Myneni, R.B., et al., 2002. Climatic control of the high-latitude vegetation greening trend and Pinatubo effect. Science 296, 1687–1689.
Manusch, C., Bugmann, H., Wolf, A., 2014. The impact of climate change and its uncertainty on carbon storage in Switzerland. Reg. Environ. Change 14, 1437. doi:10.1007/s10113-014-0586-z.
Michaletz, S.T., Cheng, D., Kerkhoff, A.J., Enquist, B.J., 2014. Convergence of terrestrial plant production across global climate gradients. Nature 512 (7512), 39–43.
Mitchell, T.D., Jones, P.D., 2005. An improved method of constructing a database of monthly climate observations and associated high-resolution grids. Int. J. Climatol. 25, 693–712.
Mu, Q., Zhao, M., Running, S.W., Liu, M., Tian, H., 2008. Contribution of increasing CO_2 and climate change to the carbon cycle in China's ecosystems. J. Geophys. Res. 113, G01018. doi:10.1029/2006JG000316.
Mu, M., Duan, W.S., Wang, B., 2003. Conditional nonlinear optimal perturbation and its applications. Nonlinear Process Geophys. 10, 493–501.
Mu, M., Duan, W., Wang, Q., Zhang, R., 2010. An extension of conditional nonlinear optimal perturbation approach and its applications. Nonlinear Processes Geophys. 17 (2), 211–220.
Nemani, R.R., Keeling, C.D., Hashimoto, H., Jolly, W.M., Piper, S.C., Tucker, C.J., Myneni, R.B., Running, S.W., 2003. Climate-driven increases in global terrestrial net primary production from 1982 to 1999. Science 300 (5625), 1560–1563.
Ni, J., 2013. Carbon storage in Chinese terrestrial ecosystems: approaching a more accurate estimate. Clim. Change 119 (3–4), 905–917.
Poulter, B., et al., 2014. Contribution of semi-arid ecosystems to interannual variability of the global carbon cycle. Nature doi:10.1038/nature13376.

Qin, X., Mu, M., 2011. Influence of conditional nonlinear optimal perturbations sensitivity ontyphoon track forecasts. Q. J. Roy Meteor. Soc. 138, 185–197.
Shao, J., et al., 2016. Uncertainty analysis of terrestrial net primary pro- ductivity and net biome productivity in China during 1901–2005. J. Geophys. Res. Biogeosci. 121, 1372–1393. doi:10.1002/2015JG003062.
Sheng, W., Ren, S., Yu, G., et al., 2011. Patterns and driving factors of WUE and NUE in natural forest ecosystems along the north-south transect of eastern China. J. Geogr. Sci. 21 (4), 651–665.
Sitch, S., Smith, B., Prentice, I.C., Arneth, A., Bondeau, A., Cramer, W., Kaplan, J., Levis, S., Lucht, W., Sykes, M., Thonicke, K., Venevski, S., 2003. Evaluation of ecosystem dynamics, plant geography and terrestrial carbon cycling in the LPJ dynamic vegetation model. Global Change Biol. 9, 161–185.
Storn, R., Price, K., 1997. Differential evolution - a simple and efficient heuristic for global optimization over continuous spaces. J. Global Optim. 11, 341–359.
Sun, G.D., Mu, M., 2011. Nonlinearly combined impacts of initial perturbation from human activities and parameter perturbation from climate change on the grassland ecosystem. Nonlinear Processes Geophys 18, 883–893.
Sun, G.D., Mu, M., 2012. Responses of soil carbon variation to climate variability in China using the LPJ model. Theor. Appl. Climatol. 110, 143–153.
Sun, G.D., Mu, M., 2013. Understanding variations and seasonal characteristics of net primary production under two types of climate change scenarios in China using the LPJ model. Clim. Change 120, 755–769.
Sun, G.D., Mu, M., 2014. The analyses of the net primary production due to regional and seasonal temperature differences in eastern China using the LPJ model. Ecol. Modell. 289, 66–76.
Sun, G.D., Mu, M., 2016. A new approach to identify the sensitivity and importance of physical parameters combination within numerical models, using the Lund–Potsdam–Jena (LPJ) model as an example. Theor. Appl. Climatol. doi:10.1007/s00704-015-1690-9.
Tao, F., Zhang, Z., 2010. Dynamic responses of terrestrial ecosystems structure and function to climate change in China. J. Geophys. Res. 115, G03003. doi:10.1029/2009JG001062.
Walker, A.P., et al., 2015. Predicting long-term carbon sequestration in response to CO_2 enrichment: how and why do current ecosystem models differ? Global Biogeochem. Cycles 29, 476–495. doi:10.1002/2014GB004995.
Wania, R., Ross, I., Prentice, I.C., 2009. Integrating peatlands and permafrost into a dynamic global vegetation model: 1. Evaluation and sensitivity of physical land surface processes. Global Biogeochem. Cycles 23, GB3014. doi:10.1029/2008GB003412.
Wania, R., Ross, I., Prentice, I.C., 2010. Implementation and evaluation of a new methane model within a dynamic global vegetation model: LPJ-WHyMe v1.3.1. Geosci. Model Dev. 3, 565–584. doi:10.5194/gmd-3-565-2010.
Wang, H., 2014. A multi-model assessment of climate change impacts on the distribution and productivity of ecosystems in China. Reg. Environ. Change 14, 133. doi:10.1007/s10113-013-0469-8.
Wang, Q., Mu, M., Dijkstra, H.A., 2012. Application of the conditional nonlinear optimal perturbation method to the predictability study of the Kuroshio large meander. Adv. Atmos. Sci. 29 (1), 118–134. doi:10.1007/s00376-011-0199-0.
Wang, Y.P., Barrett, D.J., 2003. Estimating regional terrestrial carbon fluxes for the Australian continent using a multiple-constraint approach. Tellus B 55, 270–289. doi:10.1034/j.1600-0889.2003.00031.x.
Willeit, M., Ganopolski, A., Dalmonech, D., et al., 2014. Time-scale and state dependence of the carbon-cycle feedback to climate. Clim. Dyn. 42, 1699. doi:10.1007/s00382-014-2102-z.
Wolf, A., Lazzarotto, P., Bugmann, H., 2012. The relative importance of land use and climatic change in Alpine catchments. Climatic Change 111, 279. doi:10.1007/s10584-011-0209-3.
Woodward, F.I., Lomas, M.R., 2004. Vegetation dynamics – simulating responses to climatic change. Biol. Rev. 79, 643–670. doi:10.1017/S1464793103006419.
Wu, X., Lin, X., Zhang, Y., et al., 2014. Impacts of climate change on ecosystem in priority areas of biodiversity conservation in China. Chin. Sci. Bull. 59, 4668. doi:10.1007/s11434-014-0612-z.
Yurova, A.Y., Volodin, E.M., 2011. Coupled simulation of climate and vegetation dynamics. Izv. Atmos. Ocean. Phys. 47, 531. doi:10.1134/S0001433811050124.
Zhao, M.S., Running, S.W., 2010. Drought-induced reduction in global terrestrial net primary production from 2000 through 2009. Science 329, 940–943.
Zhao, D., Wu, S., 2014. Vulnerability of natural ecosystem in China under regional climate scenarios: an analysis based on eco-geographical regions. J. Geogr. Sci. 24, 237. doi:10.1007/s11442-014-1085-3.
Zhou, T., Shi, P., Jia, G., Luo, Y., 2013. Nonsteady state carbon sequestration in forest ecosystems of China estimated by data assimilation. J. Geophys. Res. Biogeosci. 118, 1369–1384. doi:10.1002/jgrg.20114.
Zhu, Q., Zhuang, Q., 2015. Ecosystem biogeochemistry model parameterization: do more flux data result in a better model in predicting carbon flux? Ecosphere 6 (12), 283. http://dx.doi.org/10.1890/ES15-00259.1.
Zheng, Q., Dai, Y., Zhang, L., et al., 2012. On the application of a genetic algorithm to the predictability problems involving "On—Off" Switches. Adv. Atmos. Sci. 29 (2), 422–434. doi:10.1007/s00376-011-1054-z.
Zhan, X., Yu, G., He, N., Fang, H., Jia, B., Zhou, M., Wang, C., Zhang, J., Zhao, G., Wang, S., Liu, Y., Yan, J., 2014. Nitrogen deposition and its spatial pattern in main forest ecosystems along north-south transect of eastern China. Chin. Geograph. Sci. 24 (2), 137–146. doi:10.1007/s11769-013-0650-5.
Zobler, L., 1986. A World Soil File for Global Climate Modeling. NASA Technical Memorandum, 87802. NASA, Washington, D.C, p. 32.